

PACS numbers: 42.50.Gy; 32.80.–t; 42.25.Ja
DOI: 10.1070/QE2011v041n11ABEH014592

Influence of self-induced transparency on adiabatons in the lambda EIT scheme with degeneracy of levels

O.M. Parshkov

Abstract. **We present the results of numerical simulation of the adiabaton emergence process in the lambda scheme of degenerate energy levels with the quantum number of the total angular momentum, $J = 0, 2, 1$. In the case of linear polarisation of the input high-frequency field and circular polarisation of the input low-frequency field, the energy of the high-frequency component of the adiabaton is shown to focus in two or more pulses: in one of the pulses the field is circularly polarised in a direction opposite to that of the low-frequency input field, whereas in other pulses it is circularly polarised in the same direction as that of the field. This effect is caused by the specific character of electromagnetically induced transparency in the lambda scheme under study and by the trends introduced by self-induced transparency in it.**

Keywords: *electromagnetically induced transparency, self-induced transparency, adiabaton.*

1. Introduction

Electromagnetically induced transparency (EIT) occupies a worthy place among the most important effects of laser physics. The EIT principles formed the basis of substantial progress in the fields of nonlinear optics and quantum information theory [1–3], quantum communication [3–5], optical systems, quantum memory [3], high-precision magnetometry [6] and chronometry [7]. Apart from atomic and molecular systems, media, where EIT is observed, include, for example, solids with rare-earth impurities [8], quantum-well semiconductor structures [9], superconducting structures [10] and metamaterials [11]. Investigation of polarisation effects accompanying EIT in the media with degenerate quantum energy levels is the next step in studying this phenomenon. For example, in rubidium vapours with EIT, birefringence [12], magneto-chiral anisotropy [13], optical activity [14], and nonlinear Faraday effect [15] were observed.

In most EIT experiments [2, 3], there are situations that can be interpreted as formation of a special pulse structure called an adiabaton. The adiabaton theory in the case of EIT on nondegenerate quantum transitions was first proposed in [16, 17] and later refined and extended in [18, 19].

Volkov et al. [20] simulated numerically EIT in the lambda scheme of degenerate energy levels with the quantum number of the total angular momentum, $J = 0, 2, 1$. They showed that if the input high-frequency radiation is linearly polarised, and the input low-frequency field is circularly polarised, then inside the medium the high-frequency component of the adiabaton splits into two pulses with circular oppositely directed polarisations of the fields. Theory [16–19] described the adiabaton with a single high-frequency pulse, and, therefore, the authors of [20] called the considered pulse structure the double adiabaton. However, in [20], the input high-frequency pulse area was assumed smaller than the area needed for appearance of self-induced transparency (SIT) [21] in the absence of the low-frequency field. This excluded any effect of the SIT on the EIT process.

This paper presents the results of studies that extend the scope of the theory [20] by considering input high-frequency pulses, whose intensity is sufficient for the occurrence of SIT in the absence of low-frequency radiation. We have performed simulations for the lambda scheme of the ^{208}Pb isotope energy levels, where EIT of circularly polarised laser fields is observed [22]. As in [20], we take into account the level degeneracy and Doppler broadening of quantum transitions. In addition, we consider relaxation processes.

2. Formulation of the boundary problem

Consider the lambda scheme consisting of the nondegenerate ($J = 0$) lower, five-fold degenerate ($J = 2$) middle, and triply degenerate ($J = 1$) upper levels, which is formed by the $6p^2\,{}^3P_0$, $6p^2\,{}^3P_2$, and $6p7s\,{}^3P_1^o$ levels of the ^{208}Pb isotope. Let ϕ_k ($k = 1, 2, \ldots, 9$) be the orthonormalised set of common eigenfunctions of the Hamiltonian, momentum and its projection on the z axis for an isolated atom, which correspond to the lower ($k = 1$, $M = 0$), upper ($k = 2, 3, 4$, $M = -1, 0, 1$, respectively) and middle ($k = 5, 6, 7, 8, 9$, $M = -2, -1, 0, 1, 2$, respectively) levels. Here, M is the quantum number of the total angular momentum projections on the z axis. Let D_1 and D_2 be the reduced electric dipole moments for the $J = 0 \to J = 1$ and $J = 2 \to J = 1$ transitions, respectively, and ω_1 and ω_2 be the frequencies of these transitions for an atom at rest. We also assume that $T_1 = 2/\Delta_1$, where Δ_1 is the width (at the e^{-1} height level) of the density distribution of the quantum transition ($J = 0 \to J = 1$) frequencies ω_1' due to the Doppler effect.

We represent the electric field of two laser pulses propagating along the z axis with carrier frequencies ω_1 and ω_2 ($\omega_1 > \omega_2$) in the form

$$\boldsymbol{E} = \mathrm{Re}\sum_{l=1}^{2}\mu_l(\boldsymbol{e}_+ f_l + \boldsymbol{e}_- g_l)\exp[\mathrm{i}(\omega_l t - k_l x)], \qquad (1)$$

where $\mu_l = \hbar\sqrt{2l+1}/(|D_l|\,T_1)$; $\boldsymbol{e}_+ = \boldsymbol{e}_-^* = (\boldsymbol{i} + \mathrm{i}\boldsymbol{j})/2$; $\boldsymbol{i}$, $\boldsymbol{j}$ are the unit vectors of the x and y axes, respectively; f_l, g_l are the com-

O.M. Parshkov Saratov State Technical University, ul. Politekhnicheskaya 77, 410054 Saratov, Russia; e-mail: oparshkov@mail.ru

Received 25 March 2011; revision received 20 June 2011
Kvantovaya Elektronika **41** (11) 1010–1015 (2011)
Translated by I.A. Ulitkin

plex amplitudes of the right- and left-hand polarised circular components of high-frequency ($l = 1$) and low-frequency ($l = 2$) radiations, respectively, which are the functions of z and t; $k_l = \omega_l/c$. Note that in the EIT theory, high-frequency radiation is called the probe field and low-frequency radiation – the control field [2, 3].

The wave function of an atom can be written in the form

$$\Psi = \bar{c}_1\phi_1 + \left(\sum_{k=2}^{4}\bar{c}_k\phi_k\right)\exp(-\mathrm{i}\xi_1) + \left(\sum_{k=5}^{9}\bar{c}_k\phi_k\right)\exp[-\mathrm{i}(\xi_1-\xi_2)], \quad (2)$$

where $\xi_l = \omega_l - k_l z$; $l = 1, 2$. Let us introduce the c_k quantities

$$c_1 = p_1^*\bar{c}_1, \quad c_2 = \bar{c}_2, \quad c_4 = \bar{c}_4, \quad c_5 = p_2\bar{c}_5,$$

$$c_7 = (1/\sqrt{6})p_2\bar{c}_7, \quad c_9 = p_2\bar{c}_9,$$

where $p_l = 2D_l/|D_l|$. Let us define the normalised independent variables s and w as

$$s = \frac{z}{z_0}, \quad w = \frac{t - z/c}{T_1}, \quad z_0 = \frac{3\hbar c}{2\pi N|D_1|^2 T_1\omega_1}, \quad (3)$$

where N is the concentration of atoms and c is the speed of light. By describing the evolution of the field and atoms with the help of Maxwell and Schrödinger equations, respectively, we obtain, in the slowly varying amplitude approximation, the system of equations

$$\begin{aligned}
&\frac{\partial f_1}{\partial s} = \frac{\mathrm{i}}{\sqrt{\pi}}\int_{-\infty}^{+\infty} c_1 c_2^*\exp(-\varepsilon_1^2)\mathrm{d}\varepsilon_1,\\
&\frac{\partial f_2}{\partial s} = -\frac{\mathrm{i}}{\sqrt{\pi}}\xi\int_{-\infty}^{+\infty}(c_4^* c_9 + c_2^* c_7)\exp(-\varepsilon_1^2)\mathrm{d}\varepsilon_1,\\
&\frac{\partial g_1}{\partial s} = -\frac{\mathrm{i}}{\sqrt{\pi}}\int_{-\infty}^{+\infty} c_1 c_4^*\exp(-\varepsilon_1^2)\mathrm{d}\varepsilon_1,\\
&\frac{\partial g_2}{\partial s} = \frac{\mathrm{i}}{\sqrt{\pi}}\xi\int_{-\infty}^{+\infty}(c_2^* c_5 + c_4^* c_7)\exp(-\varepsilon_1^2)\mathrm{d}\varepsilon_1,\\
&\frac{\partial c_1}{\partial w} = -\mathrm{i}(f_1 c_2 - g_1 c_4),\\
&\frac{\partial c_2}{\partial w} + \mathrm{i}\varepsilon_1 c_2 = -\frac{\mathrm{i}}{4}(f_1^* c_1 + g_2^* c_5 - f_2^* c_7) - \gamma c_2,\\
&\frac{\partial c_4}{\partial w} + \mathrm{i}\varepsilon_1 c_4 = \frac{\mathrm{i}}{4}(g_1^* c_1 - g_2^* c_7 + f_2^* c_9) - \gamma c_4,\\
&\frac{\partial c_5}{\partial w} + \mathrm{i}\varepsilon_1(1-\beta)c_5 = -\mathrm{i}g_2 c_2,\\
&\frac{\partial c_7}{\partial w} + \mathrm{i}\varepsilon_1(1-\beta)c_7 = \frac{\mathrm{i}}{6}(f_2 c_2 - g_2 c_4),\\
&\frac{\partial c_9}{\partial w} + \mathrm{i}\varepsilon_1(1-\beta)c_9 = \mathrm{i}f_2 c_4,
\end{aligned} \quad (4)$$

where

$$\varepsilon_1 = T_1(\omega' - \omega_1); \quad \beta = \omega_2/\omega_1; \quad \xi = 0.75\beta|D_1/D_2|^2.$$

The amplitudes $\bar{c}_3$, $\bar{c}_6$ and $\bar{c}_8$ are not included in system (4). Their evolution is determined by a closed system of three differential equations, which, under the initial conditions $\bar{c}_3 = \bar{c}_6 = \bar{c}_8 = 0$ assumed below, has a solution $\bar{c}_3 = \bar{c}_6 = \bar{c}_8 = 0$ for all s and w. Integrals in the right-hand sides of the first four equations of system (4) are introduced to account for Doppler broadening by averaging the field-induced dipole moments of individual atoms in the parameter ε_1, which is uniquely related to the velocity of thermal motion of each atom along the z axis. In the equation for c_2 and c_4 we introduced phenomenologically the terms $-\gamma c_2$ and $-\gamma c_4$ to take into account the spontaneous decay of the upper-level states of the lambda scheme in question. Here, $\gamma = T_1/(2\tau_h)$, where τ_h is the radiative lifetime of the $6p7s\,^3P_1^o$ level. For the selected transitions of ^{208}Pb, we have, according to [23], $\beta = 0.7$, $\xi = 2.11$ and $\gamma = 1.5\times 10^{-2}$ at temperature $T = 900-1000$ K.

To present the results of calculations, we will use below the parameters a_l, α_l, γ_l of the polarisation ellipse of high- ($l = 1$) and low-frequency ($l = 2$) fields. Here, a_l is the semi-major axis of the polarisation ellipse, measured in units of μ_l; α_l is the angle of its inclination to the x axis; γ_l is the ratio of the minor axis of the polarisation ellipse to the major ($a_l \geqslant 0$, $0 \leqslant \alpha_l < \pi$, $-1 \leqslant \gamma_l \leqslant 1$ [24]). The condition $0 < \gamma_l < 1$ ($-1 < \gamma_l < 0$) means the right-hand (left-hand) elliptic polarisation, $\gamma_l = 0$ corresponds to linear polarisation, $\gamma_l = +1$ – to right-hand circular polarisation, $\gamma_l = -1$ – to left circular polarisation. If $|\gamma_l| = 1$, the angle α_l is not defined and we formally assume that $\alpha_l = -0.1$.

The initial conditions ($w = 0$) for system (4) are commonly used to find all the atoms at the lower energy level at the initial instant of time. The boundary conditions ($s = 0$) are given in the form

$$\alpha_1 = 0.5, \quad \gamma_1 = 0, \quad a_1 = a_{10}\mathrm{sech}[(w - w_{10})/\tau_{10}], \quad (5)$$

$$\alpha_2 = -0.1, \quad \gamma_2 = -1, \quad a_2 = a_{20}\{\tanh[(w - w_{21})/\tau_{20}] + \tanh[(-w + w_{22})/\tau_{20}]\}. \quad (6)$$

Equalities (5) describe a bell-shaped pulse of linearly polarised input high-frequency radiation, whose polarisation plane makes an angle of ~30° to the x axis. Equalities (6) correspond to the input low-frequency pulsed left-hand circularly polarised radiation with the envelope in the form of a pulse with a flat top, which is switched on before the arrival and switched off after the termination of the input high-frequency radiation pulse. Such a scheme for imposing the input pulses is called counterintuitive [17] and is most often used in the experimental study of EIT. The amplitudes a_{10} and a_{20} give a peak intensity of the input high-frequency pulse and the intensity of the input low-frequency pulse with a flat top. Parameters τ_{10} and w_{10} determine (in units of T_1) the duration of the input high-frequency pulse and the temporal position of its peak. Parameters τ_{10}, w_{21} and w_{22} set, respectively, the duration (in units of T_1) of the fronts of the input low-frequency pulse and temporal position of each of them ($w_{21} < w_{22}$, $\tau_{10} = w_{22} - w_{21}$).

Note that the area Θ_1 of the input high-frequency pulse (5) in terms of the SIT theory is determined by the area under the graph of the function $\sqrt{2}\,a_1(w)$ and specifies the number of 2π-pulses appearing in the medium in the absence of low-frequency radiation and relaxation [21]. As characteristics of the radiation intensity, use is also made of the fluence I_l of high- ($l = 1$) and low-frequency ($l = 2$) pulses, measured in units of $c\mu_1^2/(8\pi)$, and the energy W_1 of high-frequency radiation per unit cross section, measured in units of $c\mu_1^2 T_1/(8\pi)$.

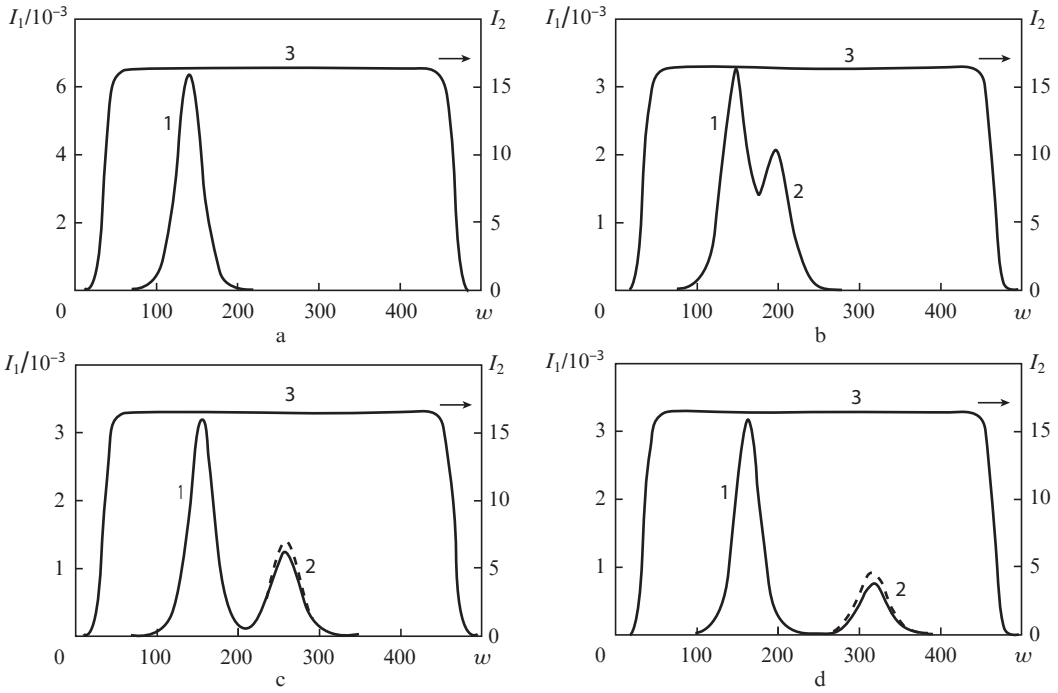

Figure 1. Evolution of the intensities I_1 and I_2 at $s = 0$ (a), 90 (b), 180 (c) and 270 (d): high-frequency components of the pulse (*1*, *2*) and a low-frequency pulse (*3*). Solid curves are plotted taking relaxation into account and dashed curved – by neglecting it.

3. Results of calculations

The first variant. We set in (5) and (6) $a_{10} = 0.08$, $a_{20} = 2.46$, $\tau_{10} = 20$, $\tau_{20} = 10$, $w_{10} = 140$, $w_{21} = 30$, $w_{22} = 470$. In this case, $\Theta_1 = 1.6\pi$, and according to the area theorem [21], in the absence of the low-frequency field and relaxation inside the medium the input high-frequency pulse must be converted to a single 2π-pulse.

Time dependences of the intensities I_1 and I_2 are shown in Fig. 1. Inside the medium, the input low-frequency radiation pulse (1 in Fig. 1a) splits into two pulses (1 and 2 in Figs 1b – d). The low-frequency radiation pulse (3 in Fig. 1) remains virtually unchanged with increasing distance s. The detailed structure of high-frequency radiation at $s = 270$ is shown in Fig. 2. One can see that the first high-frequency radiation pulse, corresponding to pulse 1 in Fig. 1d, is right-hand circularly polarised ($\gamma_1 = 1$), whereas the second pulse, corresponding to pulse 2 in Fig. 1d is left-hand circularly polarised ($\gamma_1 = -1$). The dependence of α_1 on w attests that at instants of time when polarisation is not circular, the position of the major axis of the polarisation ellipse of high-frequency radiation in the medium coincides with that of the input high-frequency pulse.

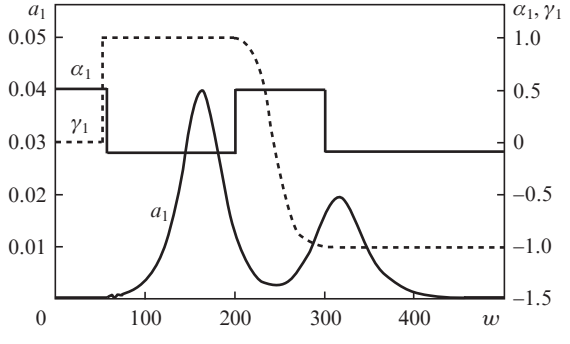

Figure 2. Evolution of the parameters of the polarisation ellipse of high-frequency radiation at $s = 270$.

The adiabaton known from the EIT theory [16–19] in the absence of degeneracy of the quantum-transition levels differs from the pulse structure, shown in Fig. 2, by the presence of a single high-frequency pulse only. In [20], the pulse structure, similar to that presented in Fig. 2, was investigated for the case $\Theta_1 = 0.8\pi$, when even in the absence of low-frequency radiation, SIT cannot appear, and was called the double adiabaton. The current calculation as well as calculations, details of which we omit, show that the double adiabaton emerges at least in cases when the area Θ_1 of the input high-frequency radiation pulse is no more than 2–3 times higher than 2π – the threshold value of the area at which SIT takes place (in the absence of low-frequency radiation).

The physical cause for formation of the two pulses in the high-frequency radiation channel was discussed in detail in [20]. Therefore, we only recall here that the right- (σ_-) and left-hand polarised (σ_+) circular components of high-frequency radiation evolve in different lambda schemes, namely, the lambda schemes of states 1, 2, 5 and 1, 4, 7, respectively. (Figure 3 shows the circular components by thin arrows and left-hand circularly polarised low-frequency radiation by thick arrows.) Difference between the electric dipole moments of 7–4 and 5–2 transitions lead to difference between the group velocities of high-frequency field components σ_- and σ_+, and, consequently, to their spatial separation.

Curve (*1*) in Fig. 4 describes the decrease in energy W_1 of the high-frequency pulse as it propagates into the medium, and curve (*2*) – the same process in the absence of relaxation ($\gamma = 0$). It is evident that relaxation has little effect on the evolution of high-frequency radiation (see dashed curves in Figs 1c, d, obtained in the absence of relaxation). This is explained by the fact known from the EIT theory [1, 2] that in the pro-

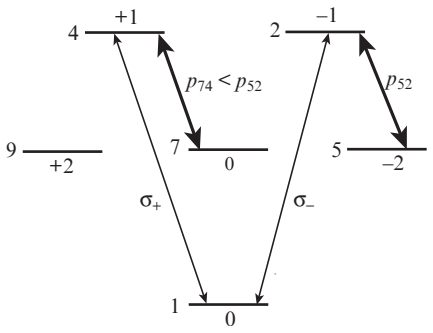

Figure 3. Scheme of quantum transitions. Numbers to the left of the horizontal lines show the number of states, the number above or below indicate the quantum number M of the states; p_{ik} is the modulus of the electric dipole moment of the corresponding transition.

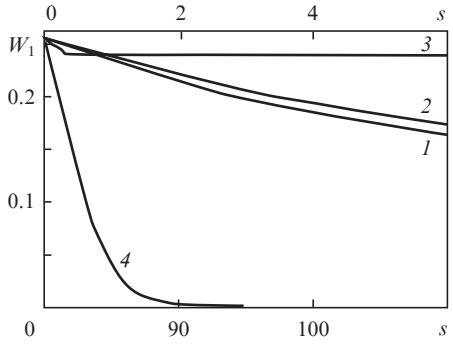

Figure 4. Dependences of W_1 on s, obtained in the presence of the low-frequency field and relaxation (*1*), in the presence of the low-frequency field without relaxation (*2*), without the low-frequency field and relaxation (*3*) and without the low-frequency field in the presence of relaxation (*4*). The lower horizontal scale is used for curves (*1–3*) and the upper – for curve (4).

cess of interaction of the fields, the upper level of the lambda scheme remains virtually unpopulated. Curve (*3*) shows the dependence of energy W_1 on s in the absence of low-frequency radiation ($a_2 = 0$) and relaxation. The constancy of W_1 in this case is due to the appearance of the 2π-pulse propagating without energy loss in the medium. Curve (*4*) illustrates the behaviour of W_1 in the absence of low-frequency field, but in the presence of relaxation. Comparison of curves (*3*) and (*4*) indicates that relaxation quickly destroys the 2π-pulse and suppresses SIT.

*The second varian*t. We set in (5) and (6) $a_{10} = 2.5$, $a_{20} = 2.46$, $\tau_{10} = \tau_{20} = 10$, $w_{21} = 30$, $w_{22} = 270$. Now, the input high-frequency pulse is twice shorter, and its peak intensity is almost 10^3 times larger than in the previous variant of calculations. In this case, $\Theta_1 = 25\pi$, so that in the absence of low-frequency radiation and relaxation in the medium twelve 2π-pulses must arise.

Time dependences of the intensities I_1 and I_2 are presented in Fig. 5. Figures 5b–d show that high-frequency radiation is concentrated in the main pulse 1 and group 2 consisting of three (as in Fig. 5d – even of four) shorter pulses. The detailed structure of high-frequency radiation at $s = 180$ is given in Fig. 6. One can see that the head high-frequency radiation pulse corresponding to pulse 1 in Fig. 5d is right-hand circularly polarised ($\gamma_1 = 1$), whereas the delayed pulses, i.e., pulses of group 2 in Fig. 5d, are left-hand circularly polarised ($\gamma_1 = -1$). Jumps up in the value of α_1 of height $\pi/2$ from the 0.5 level mean transformation of the major axis of the polarisation ellipse into the minor axis, i.e., the polarisation ellipse becomes a circle, and then again becomes an ellipse. The jumps in the opposite direction have the same meaning.

Energy redistribution between high- and low-frequency radiations leads to a significant distortion of the top of the low-frequency pulse inside the medium [see curves (*3*) in Figs 5b–d). Near the leading edge of the low-frequency pulse there appears a hump, and in the region of high-frequency

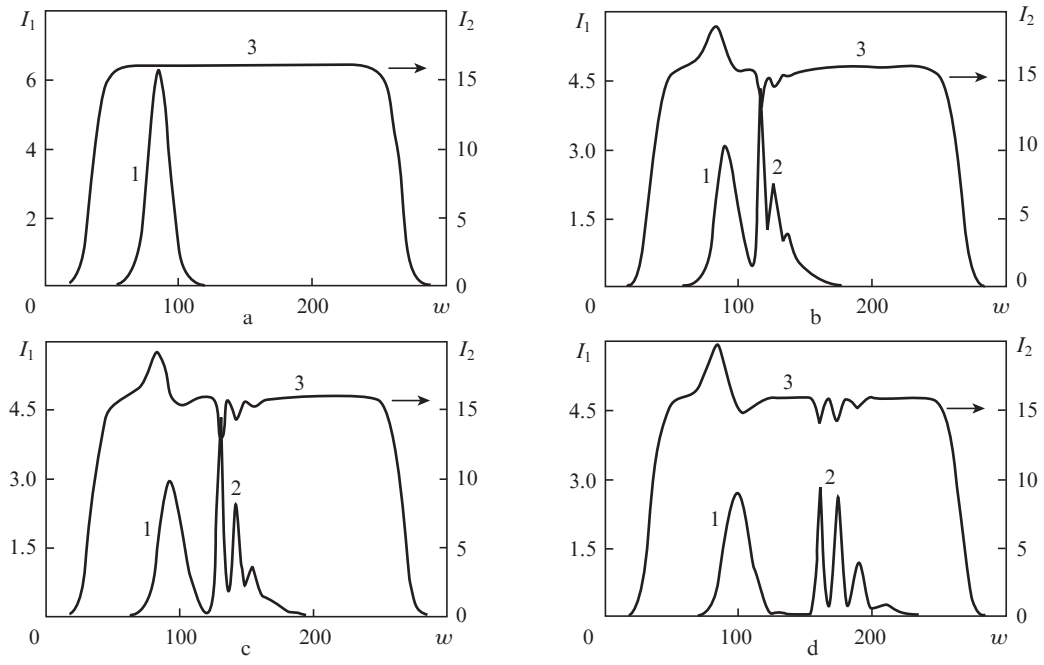

Figure 5. Evolution of the intensities I_1 and I_2 at $s = 0$ (a), 90 (b), 120 (c) and 180 (d): a head high-frequency pulse (*1*), a group of delayed high-frequency pulses (*2*) and a low-frequency pulse (*3*).

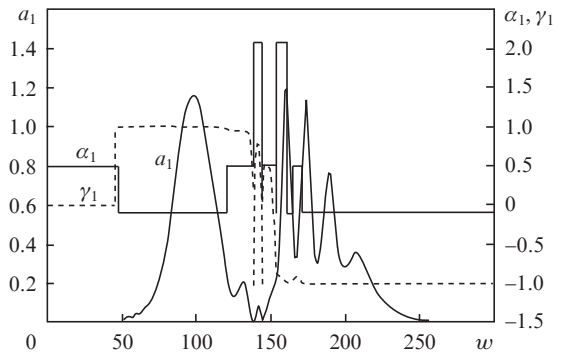

Figure 6. Evolution of the parameters of the polarisation ellipse of high-frequency radiation at $s = 180$.

radiation pulses dips are formed on the plateau of the low-frequency pulse. Because of the presence of more than two high-frequency pulses we call below the pulse structure shown in Fig. 5 the compound adiabaton. (Note that the adiabaton theory in the lambda scheme of nondegenerate transitions [16–18] predicts the formation of a hump and a single dip in the plateau of the low-frequency radiation pulse.) The detailed structure of the low-frequency radiation at $s = 180$ is presented in Fig. 7. The dependence of γ_2 on w, shown in this figure, indicates the presence of regions with a noticeable deviation from circular polarisation states. In the case when polarisation is not circular, α_2 takes the value of 0.5 or $0.5 + \pi/2$. This means that one of the axes of the polarisation ellipse of the low-frequency pulse makes the same angle with the x axis, as the plane of polarisation of the input high-frequency radiation. Note that low-frequency pulse plateau is distorted in the first variant of calculations. However, because the high-frequency pulse is weak, the distortion in Fig. 1 is imperceptible.

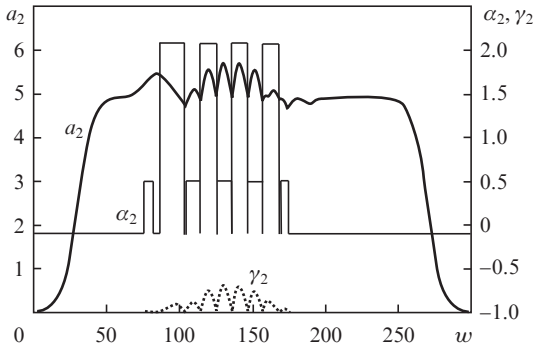

Figure 7. Evolution of the parameters of the polarisation ellipse of low-frequency radiation at $s = 180$.

Figure 8 explains the physical reason for appearance of the compound adiabaton. It shows the w dependence of the high-frequency component intensity of such an adiabaton at the initial stages of its formation ($s = 75$) and the SIT 2π-pulses, which would have been in the region of the high-frequency pulse in the absence of low-frequency radiation. Note that the region of each of the three spikes of the envelope of the adiabaton high-frequency component contains a 2π-pulse. (The far right 2π-pulse is in the region of origin of the fourth

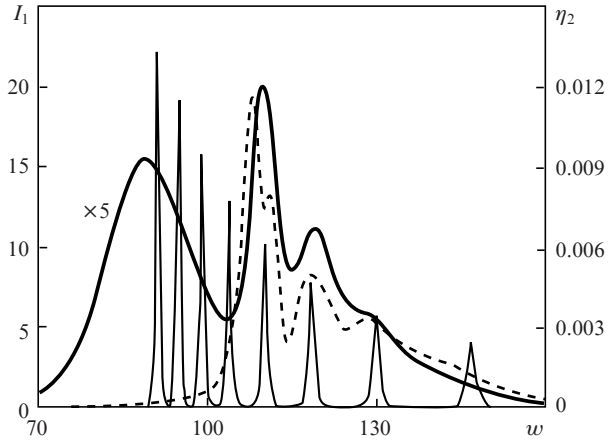

Figure 8. Intensity of the high-frequency component of the adiabaton (thick solid curve), intensities of 2π-pulses in the absence of low-frequency radiation (thin solid curve) and the mean probability of populating the states of level 4.

spike, which is weak at this distance.) This allows the process of the compound adiabaton appearance to be interpreted as influence of SIT on EIT.

The EIT effect is associated with formation of the 'dark' state [1, 2], characterised by the absence of population of the upper level in the lambda scheme. In the case of an ideal realisation of the dark state, any manifestation of SIT is not possible, because it is related to a significant population of this level. At the initial stage of adiabaton formation at the boundary conditions (5) and (6), when $\partial\Omega_2/\partial t = 0$, the state of the lambda scheme is close to dark with increasing Rabi frequency Ω_2 of the low-frequency transition [16, 17].

In the case of the lambda scheme of degenerate levels, the right-hand (left-hand) circularly polarised high-frequency component evolves into the lambda scheme of states 1–2–5 (1–4–7) (Fig. 3). Because at small distances s, low-frequency fields in both lambda schemes are the same and $p_{52} > p_{74}$, the Rabi frequency of low-frequency radiation in the lambda scheme 1–2–5 is higher than that in the lambda scheme 1–4–7. In this connection, the state of the lambda scheme 1–2–5 is closer to the dark one than that of the lambda scheme 1–4–7. Therefore, SIT does not affect the evolution of the right-hand circularly polarised high-frequency pulse of the double adiabaton formed in the lambda scheme 1–2–5. (Three left-hand 2π-pulses in Fig. 8 do not generate spikes in the envelope of the high-frequency pulse of the adiabaton.) However, the initial stage of SIT formation affects the left-hand circularly polarised high-frequency pulse of the double adiabaton produced in the lambda scheme 1–4–7 in the form of spikes on its envelope.

In the region of each spike, the value of $\partial\Omega_1/\partial t$ (Ω_1 is the Rabi frequency of the high-frequency transition) increases. According to the criterion of adiabatic approximation [16, 17], this leads to further deviation of the state of the lambda scheme 1–4–7 from the dark and to decay of the left-hand circularly polarised high-frequency component of the adiabaton to sufficiently well separated subpulses (Fig. 5d, pulses of group 2).

The dashed curve in Fig. 8 shows the w dependence of $\eta_2 = |c_4|$ – population of the upper level of the lambda scheme 1–4–7, averaged over the Doppler spread in frequency of quantum transitions. According to the dependence, distor-

tion of the envelope to the left-hand polarised high-frequency components of the adiabaton is accompanied by the transfer of ~1% of the atoms to the upper level 4 of the lambda scheme 1–4–7. Calculation also shows that the population of the upper level 2 of the lambda scheme 1–2–5 is 50 or more times less, i.e., it remains virtually unpopulated.

The role of inhomogeneous broadening of the resonance processes is known to decrease with increasing radiation intensity. On the other hand, inhomogeneous broadening leads to a decrease [2] in the effectiveness of EIT, which is responsible, in this case, for splitting high-frequency radiation of the adiabaton into right- and left-hand circularly polarised components. This explains the fact that such a splitting in the first variant of calculations takes place at a greater distance ($s \approx 180$, Figs 1b, c) than in the second variant ($s \approx 90–120$, Figs 5b, c) when high-frequency field is more intense.

4. Dimensional estimates

The most important characteristic of ^{208}Pb isotope vapours from the standpoint of experimental verification of the conclusions of the above theory is the concentration N. Another important parameter is the 'time of the inhomogeneous broadening' T_1. Both these quantities enter into formulas (3) determining the normalisation of the variables of the boundary problem. If the vapour is saturated, T_1 and N are uniquely related to each other through the absolute temperature T.

Let $N = 3.4 \times 10^{13}$ cm^{-3}, which corresponds to the saturated ^{208}Pb vapours at $T = 950$ K [25]. At this temperature, $T_1 = 1.63 \times 10^{-10}$ s. Using (3) and the data of [23] for the oscillator strengths of quantum transitions of the ^{208}Pb isotope, we find $z_0 = 0.034$ cm. Then, the duration of the input high-frequency pulses (FWHM) for the first and second variants of calculations amounts to 8 and 4 ns, and peak intensity of the pulses – to 8 and 3 kW cm^{-2}, respectively. In both variants, the intensity of the input low-frequency pulse in the region of its flat top is about 20 kW cm^{-2}, and its duration should exceed the length of the input high-frequency pulse by several times. The maximum normalised distances $s = 270$ and 180 in the first and second variants of calculations correspond to distances of ~9 and ~6 cm. In the second variant, the velocity of pulses 1 and 2 in Fig. 5 is, respectively, 14 and 77 times less than the speed of light in vacuum.

5. Conclusions

Numerical simulations have shown that when EIT appears in the lambda scheme of degenerate quantum transition, the SIT effect leads not to splitting of the high-frequency pulse into 2π-pulses but to significant changes in the pulse envelopes of adiabatons realizing EIT. The SIT influence is most clearly expressed in the splitting of one of the circularly polarised components of high-frequency radiation into subpulses. Such a modification of the adiabaton structure occurs at sufficiently strong input high-frequency pulses whose area is substantially greater than the threshold one for the SIT equal to 2π. If the area of the input high-frequency pulse slightly exceeds the threshold, SIT does not affect the structure of the adiabaton pulses and the adiabaton is qualitatively similar to the double adiabaton arising in the case when the area of the input high-frequency pulse is less than the threshold value 2π [20].

The distance at which the adiabaton with a multipulse structure of high-frequency radiation is formed, decreases with increasing intensity of the input high-frequency pulse. This is due to a decrease in the role of inhomogeneous broadening in the formation of EIT.

Note that the adiabatons considered in this paper do not retain their shape during propagation, as opposed to the adiabatons described in [16, 17]. This is explained by the fact that the authors of [16, 17] neglected such an important factor as the inhomogeneous broadening of quantum transitions.

References

1. Harris S.E. *Phys. Today*, **50**, 36 (1997).
2. Fleischhauer M., Imamoğlu A., Marangos J. *Rev. Mod. Phys.*, **77**, 633 (2005).
3. Lukin M.D. *Rev. Mod. Phys.*, **75**, 457 (2003).
4. Duan L.-M., Lukin M.D., Cirac J.I., Zoller P. *Nature (London)*, **414**, 413 (2001).
5. Sinara A. *Phys. Rev. Lett.*, **97**, 253601 (2006).
6. Martinelly M., Valente P., Failache H., Felinto D., Cruz L.S., Nussenzveig P., Lezama A. *Phys. Rev. A*, **69**, 043809 (2004).
7. Gordon A., Micalizio S., Levi F. *Phys. Rev. A*, **66**, 063807 (2002).
8. Ham B.S., Hemmer P.R., Shahriar M.S. *Opt. Commun.*, **144**, 227 (1997).
9. Nikonov D.E., Imamoğlu A., Scully M.O. *Phys. Rev. B*, **59**, 12212 (1999).
10. Abdumalikov A.A. Jr., Astafiev O., Zagoskin A.M., Pashkin Yu.A., Nakamura Y., Tsai J.S. *Phys. Rev. Lett.*, **104**, 193601 (2010).
11. Tassin P., Zhang L., Koschny T., Economou E.N., Soukoulis C.M. *Opt. Express*, **17**, 5595 (2009).
12. Tai Hyun Yoon, Chang Yong Park, Sung Jong Park. *Phys. Rev. A*, *70*, 061803(R) (2004).
13. Sautenkov V.A., Rostovtsev Yu.V., Chen H., Hsu P., Agarwal Girish S., Scully M.O. *Phys. Rev. Lett.*, **94,** 233601 (2005).
14. Bo Wang, Shujing Li, Jie Ma, Hai Wang, K.C. Peng, Min Xiao. *Phys. Rev. A*, **73**, 051801(R) (2006).
15. Drampyan R., Pustelny S., Gawlik W. *Phys. Rev. A*, **80**, 033815 (2009).
16. Grobe R., Hioe F.T., Eberly J.H. *Phys. Rev. Lett.*, **73,** 3183 (1994).
17. Grobe R., Eberly J.H. *Laser Phys.*, **5,** 542 (1995).
18. Shakhmuratov R.N., Odeurs J. *Phys. Rev. A*, **74**, 043807 (2006).
19. Hioe F.T. *Phys. Rev. A*, **78**, 063807 (2008).
20. Volkov A.V., Druzhinina N.A., Parshkov O.M. *Kvantovaya Elektron.*, **39**, 917 (2009) [*Quantum Electron.*, **39**, 917 (2009)].
21. McCall S.L., Hahn E.L. *Phys. Rev.,* **183**, 457 (1969).
22. Kasapi A., Maneesh Jain, Yin G.Y., Harris S.E. *Phys. Rev. Lett.*, **74**, 2447 (1995).
23. DeZafra R.L., Marshall A. *Phys. Rev.*, **170**, 28 (1968).
24. Born M., Wolf E. *Principles of Optics* (London: Pergamon, 1970; Moscow: Nauka, 1973).
25. Grigoriev I.S., Meilikhov E.Z. (Eds) *Handbook of Physical Quantities* (Boca Raton, NY, London: CRC Press, 1996; Moscow: Energoatomizdat, 1991).